Biosurface and Biotribology

WILEY

The Institution of Engineering and Technology

ORIGINAL RESEARCH OPEN ACCESS

Preparation and Transdermal Mechanism of Juanbi Decoction-Medicated Moxa Sticks for Joint Diseases

Yan Wang[1] | Qin Liu[1] | Yuanyuan Hu[1] | Ling Xu[1] | Rubing Wang[1] | Zhi Guo[1] | Taowei Chen[1] | Jun Zhao[1] | Song Feng[2] | Chuanrun Li[1] | Bo Wu[1]

[1]School of Pharmacy, Pharmaceutical Engineering Technology Research Center, Anhui University of Chinese Medicine, Hefei, China | [2]Anhui Guanaiyuan Traditional Chinese Medicine Biology Co. Ltd., Suzhou, China

Correspondence: Song Feng (15178269995@qq.com) | Chuanrun Li (crli@ahtcm.edu.cn) | Bo Wu (wubo@ahtcm.edu.cn)

Received: 29 October 2025 | **Revised:** 27 February 2026 | **Accepted:** 21 March 2026

Keywords: composition analysis | medicated moxa stick | network pharmacology | preparation process | transdermal mechanism

ABSTRACT

Medicated moxa sticks were prepared by mixing the herbs in Juanbi decoction with moxa wool. The components of smoke produced by combustion of these medicated moxa sticks and pure moxa sticks were analysed by gas chromatography-mass spectrometry. The smoke of the medicated moxa sticks contained 34 more active ingredients than that of the pure moxa sticks. Six of the active ingredients screened using network pharmacology and molecular docking can regulate joint diseases via the tumour necrosis factor pathway and have good binding affinities with core targets. The preparation process of the medicated moxa sticks was optimised using Box–Behnken design of response surface methodology. The smoke of the optimised product contained a high concentration of active ingredients and a low tar concentration. Molecular dynamics simulations and rat experiments demonstrated that the smoke derived from medicated moxa sticks possessed good skin permeability and detumescence activity. The developed medicated moxa sticks are environmentally friendly and show good prospects for the treatment of joint disease.

1 | Introduction

Moxibustion is a traditional Chinese medical treatment technique that benefits Qi, activates collaterals and warms the meridians [1–3]. It is suitable for bi syndrome induced by wind, cold and dampness. Its therapeutic effect is attributed to the combined effects of thermal and non-thermal radiation and pharmacological effects, with the thermal effect playing a crucial role [4]. This treatment had been used to treat arthritis, rheumatoid arthritis, hypertension and various other diseases [5–9]. When used to treat arthritis, moxibustion has shown unique benefits and remarkable efficacy. Moxibustion treatment provides pain relief and enhances the overall function and quality of life. Compared with drugs, surgery and targeted therapy, moxibustion is non-invasive, does not affect the gastrointestinal tract, can be applied directly, is cost-effective and has good patient acceptance [10–13]. Additionally, the temperature increase induced by moxibustion increases the skin's permeability to polymeric compounds [14]. To further enhance the therapeutic effect of moxibustion, Chinese herbs can be incorporated into the moxa sticks.

Aromatic Chinese herbs are traditional Chinese medicines in which volatile components are the main active ingredients. These active ingredients primarily enter the body through skin permeation and inhalation, and then exert pharmacological effects [15]. Recent pharmacological investigations have demonstrated that volatile oils, terpenes, phenols and other active ingredients that are abundant in aromatic Chinese herbs have significant anti-inflammatory and analgesic effects and effectively promote blood circulation and accelerate tissue repair [16]. These compounds also effectively improve

Yan Wang and Qin Liu contributed equally to this work.

microcirculation and relieve inflammation and pain [17]. Ma et al. [18] showed that thunder-fire moxa sticks containing aromatic Chinese herbs were more therapeutic for knee osteoarthritis than pure moxa sticks. The addition of aromatic Chinese herbs to moxa sticks greatly improves the therapeutic efficacy and increases the comfort of patients during treatment. The formulation of aromatic Chinese herbs in medicated moxa sticks and the preparation process are crucial to the therapeutic efficacy.

Juanbi decoction (JBD), which was first described in the book Medical Mind Understanding by the Qing Dynasty physician Cheng Guopeng, has historically been used for the treatment of paralysis in Chinese medicine and has the ability to disperse wind, remove dampness and relieve pain [19]. The herbs in JBD include 11 kinds such as Cinnamomi Cortex, Chuanxiong Rhizoma and Olibanum [20]. The synergistic effects of these aromatic Chinese herbs produce a potent pharmaceutical effect in the human body. Clinical data have shown that JBD can effectively reduce the joint inflammatory response, relieve joint pain and significantly improve functional recovery in rheumatoid arthritis patients [21]. Additionally, studies have shown that JBD mitigates synovial and bone erosion by suppressing the production of proinflammatory cytokines [20, 22]. Therefore, JBD has had a profound impact on the treatment of arthritis.

In the present study, we developed medicated moxa sticks JBD and investigated if the warmth of moxibustion would promote transdermal penetration of the JBD active ingredients for treatment of joint diseases. The components in smoke produced by the combustion of medicated and pure moxa sticks were analysed using gas chromatography-mass spectrometry (GC–MS). The pharmacological mechanisms of the smoke components produced by medicated moxa sticks were analysed via network pharmacology and molecular docking. We also investigated controlling the tar concentration whilst increasing the active ingredient concentration because tar is a challenging impurity in waste synthetic gas and has multiple environmental hazards [23]. To address this, the medicated moxa sticks preparation process was optimised using the Box–Behnken design (BBD) with response surface methodology (RSM). The purpose of this optimisation was to achieve a high concentration of active ingredients and a low concentration of bottom tar. The medicated moxa sticks developed in this study are environmentally friendly and contain effective pharmaceutical components. In future, this method will allow for development of efficient and safe treatment options for patients.

2 | Materials and Methods

2.1 | Materials and Reagents

2.1.1 | Materials

Cambridge filters (ø 92 mm) were obtained from Shanghai Biotech Biotechnology Co. Ltd., China. Moxa wool was obtained from Anhui Guanaiyuan Chinese Medicine Biological Co. Ltd., China. Commercial medicated moxa sticks (State Food and Drug Administration approval number: No. Z20184071 and No. Z32020252) were purchased from Anhui Lvying Pharmaceutical Co. Ltd. and Jiangsu Kangmei Pharmaceutical Co. Ltd., China. Notopterygii Rhizoma Et Radix, Angelicae Pubescentis Radix, Cinnamomi Cortex, Gentiana Macrophylla Radix, Angelicae Sinensis Radix, Chuanxiong Rhizoma, Piperis Kadsurae Caulis, Mori Ramulus, Olibanum and Aucklandiae Radix were purchased from Bozhou Kangyiyin Biotechnology Co. Ltd., China. Glycyrrhizae Radix Et Rhizoma Praeparata Cum Melle was purchased from Danbell Biotechnology Co. Ltd., China.

2.1.2 | Reagents

Huangjiu (Chinese rice wine) was puechased from Kuaiji Mountain Shaoxing Rice Wine Co. Ltd., China. Borneol, terpineol, camphor, ligustilide, d-limonene and cineole (all $\geq$ 98% pure) were purchased from Shanghai Macklin Biochemical Technology Co. Ltd., China. Physiological saline was purchased from Shandong Qidu Pharmaceutical Co. Ltd., China. Methanol (analytical purity) was obtained from Shanghai Macklin Biochemical Technology Co. Ltd.

2.1.3 | Animals

Healthy specific pathogen-free grade Sprague Dawley rats weighing 180–220 g, were purchased from Liaoning Changsheng Technology Co. Ltd. (License No. SCXK (Liao) 2020-001). The experimental protocol was approved by the Animal Ethics Committee of Anhui University of Chinese Medicine (Approval No. AHUCM-rats-2024172).

2.2 | Preparation of Medicated Moxa Sticks

Huangjiu is often used to process herbs during traditional Chinese medicine processing due to it can guide medicinal components into blood circulation, warm and unblock the meridians, facilitate the release of active ingredients and improve drug permeability and stability [24]. The preparation process of the medicated moxa sticks is shown in Figure 1. First, 20 g of moxa wool was mixed with 2 g of Huangjiu (15% alcohol), giving a solid liquid of 10:1. The mixture was left to stand for 3 h and then the wool was dried for a predetermined period (1–4 h) at a predetermined temperature (35°C–65°C) for subsequent use. Next, 5 g of powdered Chinese herbs was added to the treated moxa wool. Huangjiu (15% alcohol, 2.5 g) was added and the mixture was left to stand for a further 3 h. The resulting mixture was dried at a predetermined temperature (35°C–65°C) for a predetermined period (1–4 h) to obtain the final moxibustion material. Finally, the moxibustion material was wrapped in mulberry paper to produce a medicated moxa stick. The solid–liquid ratio ($R_{s/l}$, g/g), drying time (t_d, h) and drying temperature (T_d, °C) were used to control the active ingredients and tar concentration.

2.3 | Collection of Combustion Smoke and Tar From the Moxa Sticks

A moxa stick (1.5 × 20 cm) was ignited, and the smoke was collected in 50 mL of methanol solution until the stick was completely burnt. Subsequently, the methanol was analysed by GC–MS. The tar produced by the medicated moxa sticks combustion was compared with that produced by pure moxa sticks and commercial medicated moxa sticks. The tar concentration produced by moxa sticks combustion was determined by the gravimetric method [25]. Cambridge filter were used to capture the moxa smoke, and the change in mass of the filter was used to calculate the tar concentration. The combustion gas and tar collection and analysis processes are shown in Figure 2.

The components of smoke produced by moxa sticks combustion were examined using GC–MS (7890 B GC system, 5977 A mass spectrometer, Agilent Technologies Inc.). The stationary phase was a modified polyethylene glycol capillary column (30 m × 0.25 mm and 0.25 μm) purchased from Abel Industries Ltd., Canada. The column temperature was maintained at 40°C for 3 min, then increased to 220°C at 5°C/min (held for 4 min) and finally increased to 280°C at 15°C/min (held for 3 min). The injector temperature was set to 280°C and the detector temperature was maintained at 280°C. A split ratio of 2:1 was used and 0.5 μL of both the reference solution and the test sample were injected. The ion source temperature was 230°C, the solvent delay was 4 min and the scan range was m/z 19–600.

2.4 | Network Pharmacology and Molecular Docking

2.4.1 | Active Ingredients and Target Screening

The identified main components were entered into the TCMSP database (https://old.tcmsp-e.com/tcmsp.php) and the SwissADME database (http://www.swissadme.ch/) for preliminary screening [26]. For the TCMSP database, compounds with oral bioavailability ≥ 30% and drug-like properties ≥ 0.18 were selected. For the SwissADME database, only with gastrointestinal absorption classified as 'High' were selected. For these compounds, seven pharmacokinetic or inhibition-related parameters (blood–brain barrier permeaation, P-glycoprotein substrate, cytochrome P450 [CYP] 1A2 inhibition, CYP2C19 inhibition, CYP2C9 inhibition, CYP2D6 inhibition and CYP3A4 inhibition) were considered and compounds with three or more 'yes' results were selected. Compounds meeting either the TCMSP or SwissADME requirements were retained for further analysis. The target of the retained compound was searched and predicted using the Swiss target prediction (http://www.swisstargetprediction.ch/) website, and the targets with a probability > 0 were

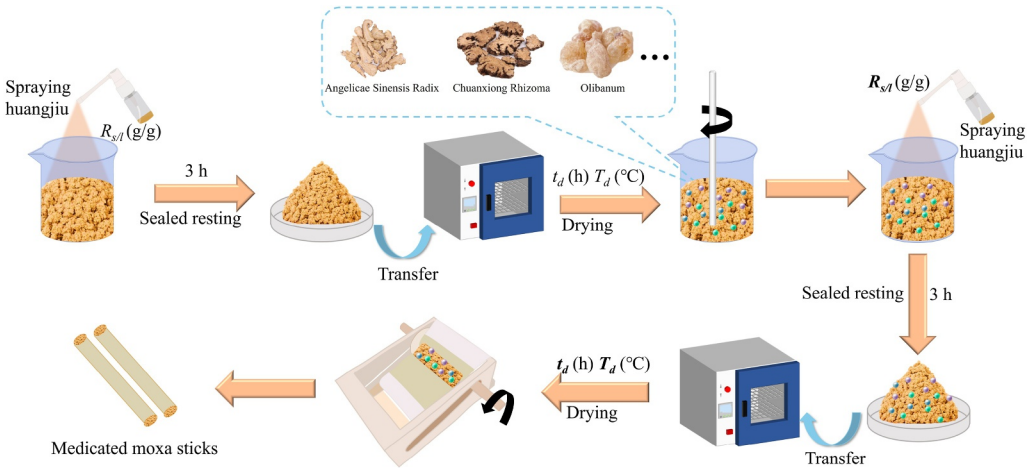

FIGURE 1 | Preparation process of medicated moxa sticks.

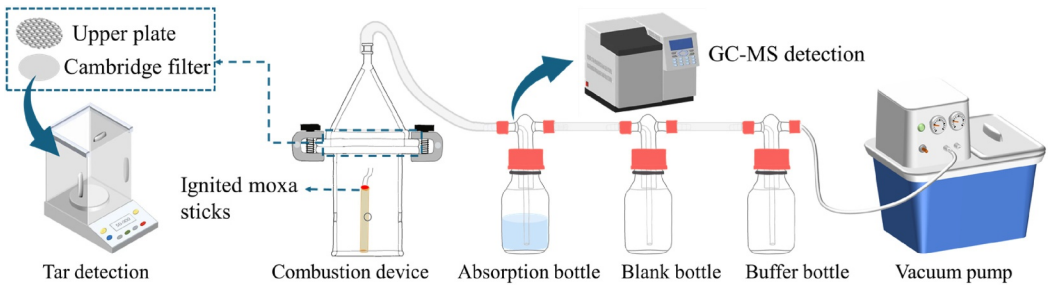

FIGURE 2 | Flue gas and tar collection and analysis.

retained. The UniProt (https://www.uniprot.org) database was used to standardise the target names.

2.4.2 | Joint Disease Targets

The GeneCards database (https://www.genecards.org/) and OMIM (https://omim.org/) database were searched for the keyword 'joint disease' for disease genes.

2.4.3 | Screening of Drug–Disease Targets and Construction of the Active Ingredient–Target–Disease Network

The Veeny 2.1.0 platform was applied to integrate active ingredient targets with the disease targets to obtain the intersection targets. The 'component-target' network of medicated moxibustion smoke was constructed by Cytoscape software.

2.4.4 | Construction of Protein–Protein Interaction Networks

The intersected gene targets were entered into the STRING (https://www.string-db.org/) database and the protein–protein interaction network was constructed. The output files were further analysed using Cytoscape software [27, 28]. Three topological attribute parameters were selected as the screening conditions for the core nodes, and targets with values greater than the respective median values were retained to finally obtain the core targets for the treatment of joint disease with the medicated moxibustion smoke.

2.4.5 | Enrichment Analysis

Gene Ontology (GO) and Kyoto Encyclopedia of Genes and Genomes (KEGG) were used to carry out enrichment analysis to obtain insight into the functions of genes and their roles in biological pathways. The results indicate the pathways in which the genes are involved and the roles they play in those pathways and can provide important clues to reveal complex biological phenomena and mechanisms. GO and KEGG enrichment analyses were performed using an online bioinformatics platform (https://www.bioinformatics.com.cn) [29].

2.4.6 | Molecular Docking Validation

Protein Data Bank files corresponding to the three-dimensional structures of the six active components were retrieved. The components and their respective targets were imported into AutoDock Tools for docking simulation calculations, and the binding abilities between the ligands and receptors were determined from the results. If the binding energy is less than 0 kcal/mol, it confirms that a component and target can spontaneously bind. If the binding energy is less than or equal to −5.0 kcal/mol, it indicates that the binding affinity between the component and target is favourable [30]. The molecular docking results were imported into PyMOL software for three-dimensional visualisation mapping and into Discovery Studio software for two-dimensional visualisation mapping.

2.5 | RSM Design

In the RSM design, $R_{s/l}$ (X_1), t_d (X_2) and T_d (X_3) were selected as variables. Discrete coding levels for the design variables were determined by referencing the most pronounced ranges of variability identified through the outcomes of univariate experiments (Table 1). RSM was used to optimise the preparation process of the medicated moxa sticks. Design-Expert 13 statistical software was used to construct a regression model for the experimental data (Equation 1) to evaluate the validity of the response model.

$$Y = \beta_0 + \sum_{i=1}^{n} \beta_i X_i + \sum_{i=1}^{n} \beta_{ii} X_i^2 + \sum_{i} \sum_{<j=2}^{n} \beta_{ij} X_i X_j, \quad (1)$$

where Y is the predicted response (Equation 2), β_0 is a constant, X_i is the linear coefficient, X_{ij} is the interaction coefficient and β_{ii} is the quadratic coefficient.

$$Y = \frac{E_i}{E_t}, \quad (2)$$

where E_i is the active component concentration (%) and E_t is the tar concentration (g/g). A higher Y value is a better result.

2.6 | Models of Molecular Dynamics Simulation

To simulate the transdermal behaviour of six active ingredients in moxa stick combustion smoke, a skin stratum corneum model was established using Materials Studio software as shown in Figure 3a. The model was mainly composed of ceramides, free fatty acids and cholesterol, which were the major lipid components in the stratum corneum. These ingredients were set at a molar ratio of 1:1:1 [29]. Molecular models of the six active ingredients of terpineol, borneol, camphor, ligustilide, d-limonene and cineole were constructed as presented in Figure 3b. A transdermal simulation system model with a size of 45 × 34 × 104 Å was finally constructed as illustrated in Figure 3c. A 20 Å vacuum layer was added along the Z direction to reduce the interference of periodic boundary conditions on intermolecular interactions. Geometric optimisation was carried out using the COMPASS force field to achieve a fully relaxed state. After optimisation, 1000 ps molecular dynamics

TABLE 1 | Coding levels of independent variables for the Box–Behnken design.

		Range and levels of independent factors		
Factors	Symbol	−1	0	1
$R_{s/l}$ (g/g)	X_1	20	15	10
t_d (h)	X_2	1	2	3
T_d (°C)	X_3	35	45	55

simulations were performed at 310.15 K and 1 atm with the Berendsen thermostat and barostat. The interaction patterns between pharmacodynamic molecules and the skin stratum corneum were systematically analysed. The transdermal penetration mechanism of these active ingredients from moxa stick combustion smoke was further explored.

2.7 | Evaluation of Transdermal Penetration of Active Components

2.7.1 | Preparation of Rat Skin

The rats were first anesthetised and there abdominal hair was removed using a depilatory cream. Next, the rats were euthanised by exsanguination from the common carotid artery. This was followed by dissection of abdominal skin. Subcutaneous fat, connective tissues and blood vessels were excised from the dissected skin [31]. Intact and undamaged skin samples were selected, rinsed with physiological saline, dried and then wrapped in aluminium foil. The skin samples were stored in a low-temperature environment at −20°C and used within 1 month [32]. Before used, the skin samples were thawed and soaked in physiological saline to restore physiological state at room temperature slowly, and then blotted dry on the surface prior to use in vitro transdermal experiments.

2.7.2 | In Vitro Transdermal Experiments

In vitro transdermal experiments were performed in a transdermal absorption device (Figure 4) using a vertical Franz diffusion cell with a receptor compartment volume of 8.0 mL and a contact area of 3.14 cm^2. The prepared rat skin was fixed on the Franz diffusion cells with the stratum corneum facing the donor compartment and the dermis in full contact with the receptor solution. A magnetic stir bar was placed inside the receptor compartment and the temperature of the receiving solution in the transdermal device was maintained at 37°C. After 40 min, 2 h, 4 h, 6 h, 8 h and 12 h, the receptor solution was collected and passed through a 0.45 μm microporous membrane filter. A 1 μL aliquot of the filtrate was withdrawn for gas chromatography analysis. Moreover, skin samples were collected at 10, 20, 30 and 40 min, respectively. The collected skin were washed three times with PBS buffer, and stored frozen in a −80°C refrigerator for 12 h. Skin tissue sections were then prepared using a cryostat at −20°C, and the sections were

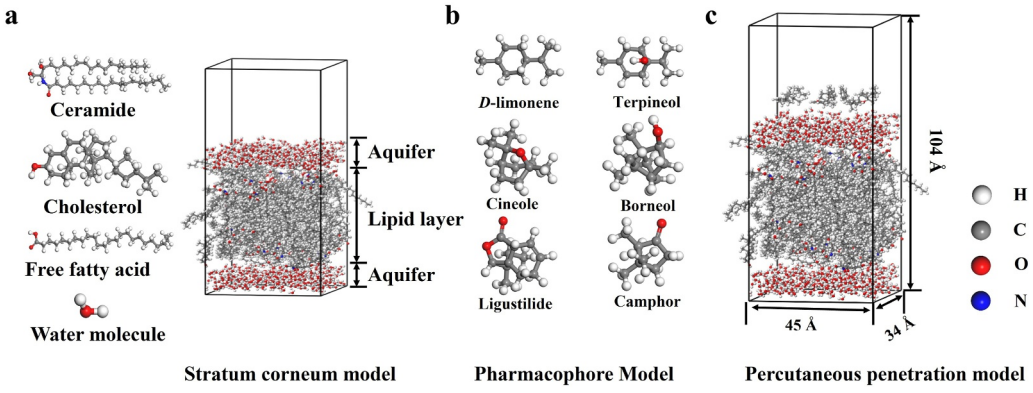

FIGURE 3 | Molecular simulation models. (a) Stratum corneum, (b) active pharmaceutical molecules and (c) transdermal simulation.

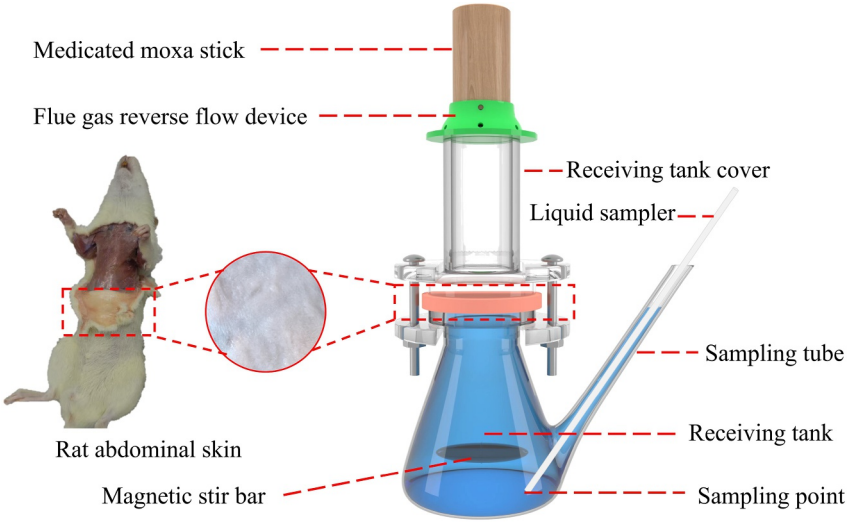

FIGURE 4 | Device for transdermal absorption.

observed and analysed under an inverted fluorescence microscope.

2.8 | In Vivo Animal Experiments

2.8.1 | Model Preparation

After 1 week of adaptive feeding, male SD rats were randomly divided into four groups with each group consisted of six rats. The groups were a blank group, a model group, a pure moxa stick treatment group and a medicated moxa stick treatment group. Rats in the model group, pure moxa stick treatment group and medicated moxa stick treatment group were subcutaneously injected with Complete Freund's adjuvant (CFA) at the tail base and right hind toe. The injection volume was 0.1 mL per site to establish the swelling model. The rats were observed continuously for 3 days after injection. Modelling was considered successful when the rat toes and ankle joints showed different degrees of redness and swelling [33, 34]. Rats in the blank group were subcutaneously injected with the same volume of normal saline at the same sites. All other procedures were consistent with those of the model groups.

2.8.2 | Intervention Methods

According to the animal acupoint standards in *Experimental Acupuncture*, rats in the pure moxa stick treatment group and medicated moxa stick treatment group were treated at the Zusanli acupoint on the right hind limb. Mild moxibustion was applied starting on the fourth day after model establishment. A moxibustion jar with a smoke reflux device was used for the treatment. The moxa stick was positioned 3–5 cm above the skin surface. This allowed the heat and moxa smoke to fully act on the local acupoint area. Each treatment session lasted 20 min. The procedure was performed once daily for 7 consecutive days [35].

2.8.3 | Evaluation of Toe Joint Swelling Degree

The day after each intervention, the toe volume of the right hind paw was measured for all rats in each group. Before measurement, a mark was placed at the rat's ankle joint. The toe volume of the right hind limb was determined using a toe volume metre (PV-200). Each rat was measured three times consecutively. The average of the measurements was used as a quantitative index to evaluate the swelling degree of the toe joints of each group.

3 | Results and Discussion

3.1 | Components in Smoke Produced by Moxa Sticks Combustion

Total ion flow diagrams of the methanol extracts of the medicated and pure moxibustion smoke were obtained using GC–MS (Figure 5). Comparison with the NIST mass spectrometry database and relevant literature was used to identify 84 components in the medicated moxibustion smoke (Supporting Information S1: Table S1) and 45 components in the pure moxibustion smoke (Supporting Information S1: Table S2).

3.2 | Network Pharmacology Analysis and Molecular Docking Results

3.2.1 | Network Pharmacology Analysis

The 84 components in the medicated moxibustion smoke were imported into the TCMSP database. Twenty-nine components that did not meet the conditions were eliminated, which left 55 active ingredients (Supporting Information S1: Table S3). After integrating the target proteins of 55 active ingredients, the Uniprot database was applied to query gene names of the target proteins and 422 active ingredient targets were obtained. For the smoke of pure moxa stick, after importing into the TCMSP database, 24 components that did not meet the conditions were

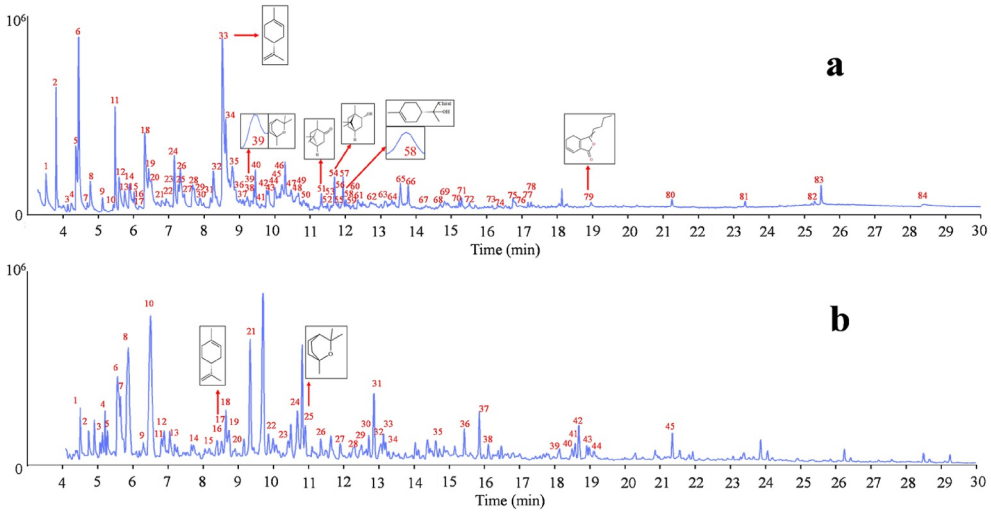

FIGURE 5 | Total ion flow diagrams for (a) medicated moxibustion smoke and (b) pure moxibustion smoke.

eliminated, which left 21 active ingredients (Supporting Information S1: Table S4). These results show that the medicated moxibustion smoke contained more active ingredients. Therefore, this smoke may have a wider range of potential pharmacological effects than pure moxibustion smoke. Next, we conducted a network pharmacology analysis of the active ingredients in the medicated moxibustion smoke.

The GeneCards and OMIM databases were used to retrieve targets associated with joint disease. Merging and removal of duplicated genes resulted in 2431 gene targets associated with joint disease (Figure 6a), which may serve as therapeutic targets for the management of joint diseases. To further elucidate the shared therapeutic targets between the bioactive compounds in medicated moxibustion smoke and joint disease–related pathways, a Venn diagram analysis was conducted. The findings revealed 123 overlapping targets (Figure 6b), indicating potential synergistic effects or common mechanisms of action. An 'active ingredient-target' regulatory network was constructed using 55 active ingredients and 123 targets related to joint disease (Figure 6c). Topological attribute analysis of the protein–protein interaction network was conducted using Cytoscape software (Figure 6d).

The median values of betweenness centrality, closenesscentrality and degree were used to screen the core targets. The analysis yielded 44 core targets (Supporting Information S1: Table S5). Thirteen core targets were from six active ingredients,

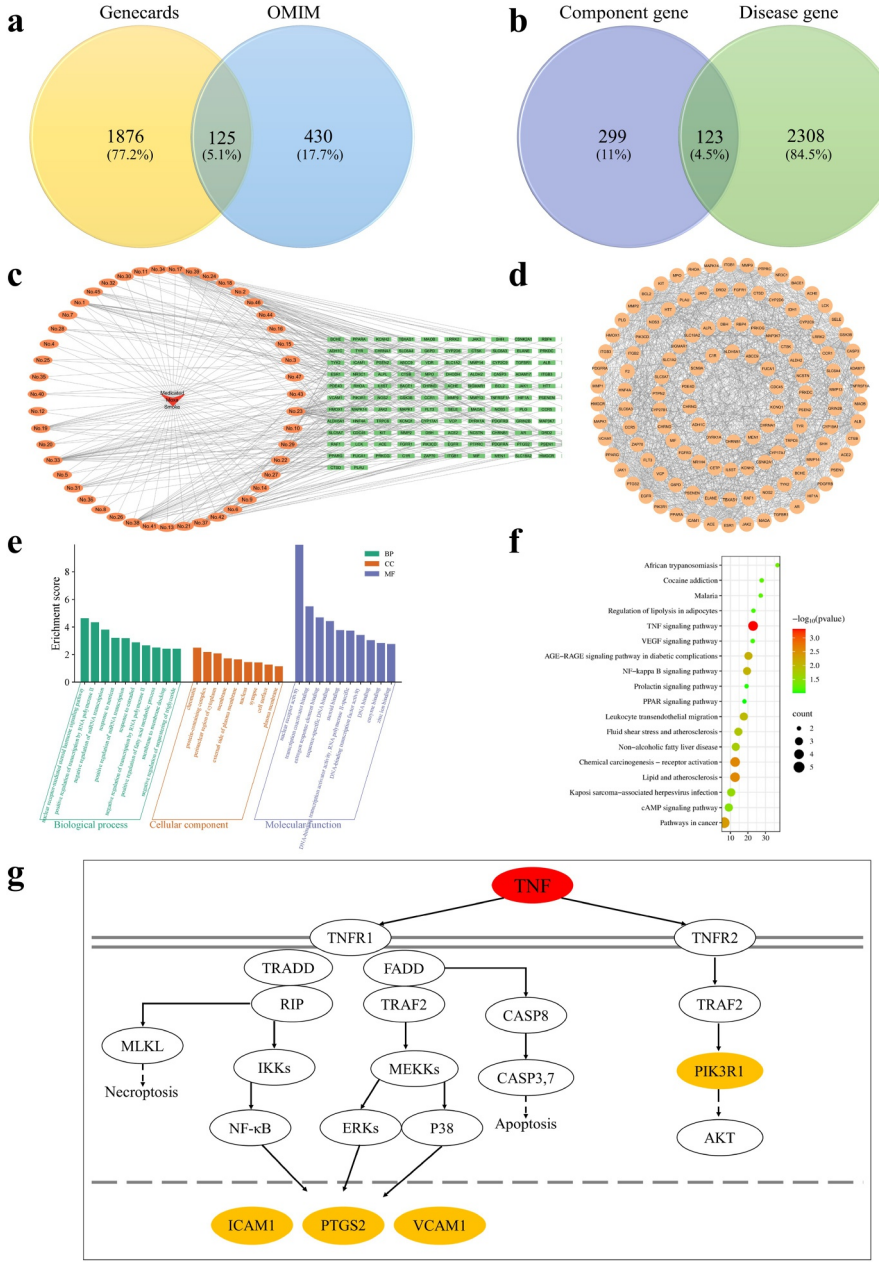

FIGURE 6 | Network pharmacology analysis. (a) Intersection of joint disease targets, (b) intersection of active ingredients and joint disease targets, (c) active ingredient target regulation network, (d) protein–protein interaction network diagram from Cytoscape software, (e) GO enrichment analysis diagram, (f) KEGG enrichment analysis map and (g) schematic diagram of the tumour necrosis factor signalling pathway.

namely terpineol, borneol, camphor, ligustilide, d-limonene and cineole. The network topology parameters of the active ingredients-related targets and the corresponding peak area percentages detected by GC–MS are shown in Table 2. It means that these six active ingredients are potential targets for the treatment of joint disease.

Signalling pathway enrichment analyses were performed on the intersected genes in Table 2. The top 10 results of GO enrichment analyses for biological processes, cellular components, molecular functions and the number of targets enriched were plotted in bar charts (Figure 6e). The results showed that the mode of drug action of the six active ingredients was related to the nuclear receptor-mediated steroid hormone signalling pathway, chromatin and nuclear receptor activity. The top 20 results of KEGG enrichment analysis were plotted as bubble plots (Figure 6f).

Treatment of joint disease may act through the tumour necrosis factor (TNF) pathway (Figure 6g), pathway in cancer and NF-κB pathway. Previous studies have demonstrated that pathway in cancer are highly regulated in synovial tissues of patients with joint disease [36]. These findings suggest that synovial tissues in joint disease exhibit tumour-like properties; therefore, pathway in cancer might serve as potential targets for the treatment and diagnosis of joint disease. TNF is involved in the inflammatory response of local tissues, primarily because of its promotion of inflammatory substances represented by NLRP3 vesicles [37, 38]. Previous research has shown that inhibition of the NF-κB pathway attenuates destructive effects of cartilage in a murine osteoarthritis model [39]. Our results suggest that the six identified active ingredients can modulate metabolic pathways associated with joint disease.

Because the TNF pathway in Figure 6f had the lowest *p*-value and highest significance among the pathways, we selected it for target analysis. From this analysis, the main targets for the action of the active ingredients were ICAM1, PIK3R1, PTGS2 and VCAM1 (Figure 6g). ICAM-1 is a transmembrane protein containing 505 amino acids and is widely found on the surface of a variety of cells. Its polymorphism is associated with susceptibility to joint disease [40]. Studies had shown that ICAM1 greatly affects the pathogenesis of joint diseases, and it is expressed in the invasion and metastasis of various malignant tumours [41]. PIK3R1 is a negative regulator of PI3K/Akt/mTOR signalling. Lipopolysaccharide down-regulates its expression and contributes to inflammation progression [42, 43]. MiR-155 can target and downregulate PIK3R1 expression, which in turn activates PI3K/Akt signalling and promotes chondrocyte apoptosis [44]. PTGS2 is a key enzyme that catalyses the rate-limiting step in the synthesis of several inflammatory prostaglandins [45]. This leads to bone destruction by promoting abnormal fibroblast-like synoviocytes proliferation and migration [46]. Additionally, it regulates angiogenesis, apoptosi and cytokine expression, all of which are down-regulated to attenuate the inflammatory response and joint disease [47]. VCAM-1 is closely related to the pathogenesis of joint disease. Relevant studies have demonstrated that it plays

TABLE 2 | The network topology parameters of the active ingredients-related targets and the corresponding peak area percentages detected by GC–MS.

No.	Name	Core target	Degree	Betweenness	Closeness	Peak area %
1	Terpineol	AR	24	101.61	0.51	0.34
		ESR1	56	678.01	0.62	
		ACHE	24	619.23	0.54	
		DRD2	20	101.03	0.51	
		PPARG	53	741.83	0.62	
		PPARA	25	97.56	0.52	
		NR3C1	31	112.18	0.55	
2	Borneol	AR	24	101.61	0.51	1.34
		ESR1	56	678.01	0.62	
		NR3C1	31	112.18	0.55	
		DRD2	20	101.03	0.51	
3	Camphor	AR	24	101.61	0.51	0.79
4	Ligustilide	CTSB	27	143.27	0.52	0.38
		ICAM1	51	203.05	0.59	
		VCAM1	47	145.00	0.58	
		PTGS2	52	456.25	0.62	
		MAOA	28	507.11	0.55	
		PIK3R1	31	75.06	0.52	
5	D-limonene	PPARA	25	97.56	0.52	9.93
6	Cineole	ACHE	24	619.23	0.54	0.47

an important role in the activation and release of immune cells in the early inflammatory response process [48, 49]. VCAM-1 can mediate the infiltration, adhesion and transendothelial movement of inflammatory cells, which are an important factors leading to the development of synovial inflammation. The above network pharmacological predictions illustrate the potential of the six active ingredients in the management of joint disease.

In this paper, six active ingredients with therapeutic effects on joint disease were identified (Table 3). Network pharmacological predictions indicated that these six active ingredients can modulate metabolic pathways associated with joint disease via pathways such as TNF signalling pathway, pathway in cancer and NF-κB signalling pathway. These six active ingredients show unique and important effects in joint disease treatment. For example, cineole and terpineol in herbal essential oils can inhibit the expression of TNF, interleukin-6 and interleukin-1 and show significant anti-inflammatory activity [50]. Ligustilide is promising for the treatment of migraine and rheumatoid arthritis pain because of its unique analgesic properties [51]. Borneol demonstrates favourable efficacy in anti-inflammatory, analgesic and antibacterial applications [52, 53]. Camphor has analgesic and anti-injury properties and is an effective ingredient for arthritis pain relief [54, 55]. D-limonene has anti-inflammatory, antibacterial and anti-injury properties and can be used to treat arthritis [56–59]. El-Ghffar et al. [60] found that cineole reduced synovial joint inflammation and improved antioxidant defence systems.

3.2.2 | Molecular Docking Results

The six active ingredients were subjected to molecular docking with the core target proteins (Supporting Information S1: Table S6). Sixteen ligand–receptor pairs had binding energies of ≤ -5.0 kcal/mol, which indicated that these molecular pairs had favourable binding potentials. According to previous research [30], target proteins and active ingredients with binding energies of ≤ -6 kcal/mol were selected for mapping (Table 4). From the results, we observed that ligustilide and CTSB were connected to the LYS-18 amino acid residue via one hydrogen bond; terpineol and AR were linked to the GLU-193 and LYS-194 amino acid residues through two hydrogen bonds; borneol and AR were connected to the LEU-195 and GLN-192 amino acid residues by two hydrogen bonds; terpineol and PPARA were connected to the GLU-91, GLN-24 and MET-25 amino acid residues through four hydrogen bonds and ligustilide and PTGS2 were connected to the ASN-43 and ARG-44 amino acid residues via two hydrogen bonds.

3.3 | Effects of Single Variables

It is well known that numerous parameters can have significant and variable effects on the preparation process. These parameters include, but are not limited to, the solid–liquid ratio, drying time, drying temperature and ultrasonication power, each of which play a crucial role in the preparation process [61–63]. In view of the importance of these parameters and their complex interactions with each other, the three most critical parameters (solid–liquid ratio, drying time and drying temperature) were selected and a series of one-factor experiments were carried out to investigate their effects separately. The results are shown in Figure 7.

3.3.1 | Solid–Liquid Ratio

The effect of the solid–liquid ratio on the preparation process was directly correlated with the tar and active ingredient concentrations. As the solid–liquid ratio was gradually adjusted from 20 to 5 g/g, the Y variable first increased and then decreased (Figure 7a). This trend indicates that the tar concentration decreased and then increased. At the same time, the active ingredients concentration first increased and then decreased. The lowest tar concentration and highest active ingredients concentration occurred when the solid–liquid ratio was 15 g/g. The results for the active ingredients were attributed to optimisation of the dissolution of the active ingredients in the solvent with an appropriate solid–liquid ratio. However, when the solid–liquid ratio was increased beyond 15 g/g, the excess solvent led to excessive dilution of the active ingredients and a decrease in their concentration [64]. The change in the tar concentration, may be closely related to the amount of Huangjiu added and the degree of protein degradation. As the solid–liquid ratio increased, the amount of Huangjiu added increased, which accelerated the protein degradation process to a certain extent and led to an initial decrease in the tar concentration. However, when the

TABLE 3 | Active ingredients in moxibustion smoke for the treatment of joint disease.

Name	Chemical structure	Pure moxibustion smoke	Medicated moxibustion smoke
Terpineol		−	+
Borneol		−	+
Camphor		−	+
Ligustilide		−	+
D-limonene		+	+
Cineole		+	+

Note: − Not present; + present.

TABLE 4 | Molecular docking binding energies and visual diagrams.

Active ingredients	Target protein	Binding energy (kcal/mol)	Visual diagram
Terpineol	AR	−6.08	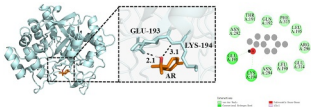
	PPARA	−6.35	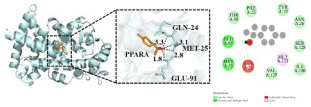
Ligustilide	CTSB	−6.92	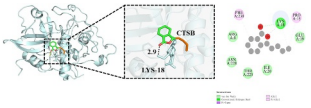
	PTGS2	−7.0	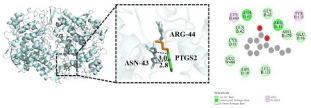
Borneol	AR	−6.08	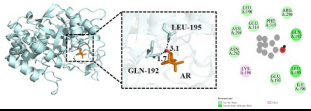

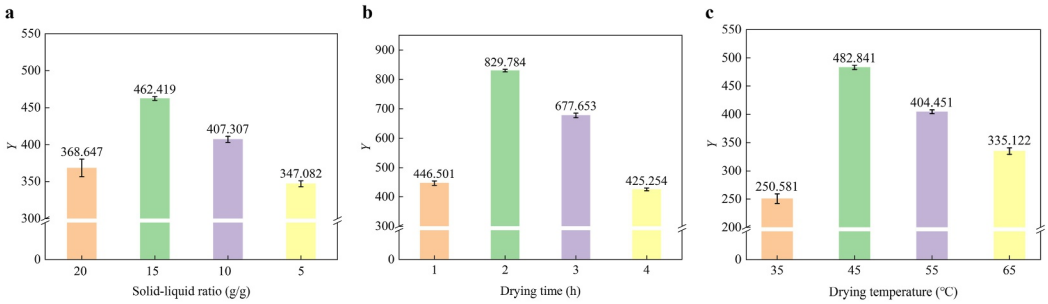

FIGURE 7 | Influence of independent variables on dependent variables. (a) Solid–liquid ratio, (b) drying time and (c) drying temperature.

solid–liquid ratio exceeded 15 g/g, the protein degradation process was excessive and more tar precursor substances were released. These precursor substances would be further transformed in the subsequent preparation process, which eventually resulted in the tar concentration increasing again [65, 66].

3.3.2 | Drying Time

The effect of drying time on the *Y* is shown in Figure 7b. As the drying time increased, the value of *Y* initially increased to a peak at 2 h and then decreased. This trend showed that the tar concentration first decreased and then increased. At the same time, the concentration of active ingredients first increased and then decreased. The increase in the concentration of active ingredients was attributed to gradual removal of water during the early stages of drying, resulting in increased volatilisation of the active ingredients from the herbs. However, when the drying time was $>$ 2 h, excessive drying of the herbs would lead to degradation of the active ingredients and decrease their concentrations in the smoke [67]. The changes in tar concentration were likely related to changes in enzyme activity in Huangjiu. In the early stage of drying, the enzyme activity may have increased because the conditions were favourable. However, as the drying process continued, the decreasing water content may inhibit enzyme activity and result in a gradual decrease in the enzyme activity [65, 68].

3.3.2.1 | Drying Temperature. The effect of the drying temperature on the *Y* is shown in Figure 7c. The value of *Y* first increased steadily as the drying temperature was increased, reached a maximum value at 45°C and then decreased. This trend showed that the tar concentration decreased and then increased. At the same time, the concentration of active ingredients increased and then decreased. In the initial stage of temperature increase, the concentration of active ingredients increased. This was attributed to the fact that a suitable temperature increased the release of the active ingredients from the herbs into the smoke. The decrease in the concentration of active ingredients when the temperature exceeded 45°C was attributed to degration of the components at high temperatures [69]. The changes in the tar concentration were also attributed to changes in the enzyme activity in the Huangjiu. Initially, as the temperature increased, the enzyme activity would increased to promote enzymatic reactions that reduce the tar concentration. However, as the temperature continued to

increase, thermal denaturation of the enzymes would lead to a decrease in enzymatic activity. Consequently, tar-forming reactions would resume and the tar concentration would increase [65, 70].

3.3.2.2 | BBD. A mathematical model was constructed using a BBD. The factors and levels for the response surface experiments are shown in Table 5. Regression analysis was conducted on the experimental results using Design Expert 8.6 and gave the following regression equation:

$$Y = 14.08 - 0.8996X_1 + 0.6068X_2 - 0.2411X_3 - 0.0783X_1X_2 - 0.8385X_1X_3 - 2.32X_2X_3 + 0.4990X_1^2 - 0.0316X_2^2 - 0.3352X_3^2. \quad (3)$$

TABLE 5 | Response surface methodology experimental design and responses.

Run	X_1 (g/g)	X_2 (h)	X_3 (°C)	Y
1	10:1 (1)	3 (1)	45 (0)	359.294
2	15:1 (0)	2 (0)	45 (0)	368.928
3	20:1 (−1)	1 (−1)	45 (0)	364.355
4	15:1 (0)	2 (0)	45 (0)	339.590
5	10:1 (1)	2 (0)	55 (1)	303.238
6	20:1 (−1)	2 (0)	35 (−1)	367.222
7	20:1 (−1)	3 (1)	45 (0)	402.586
8	15:1 (0)	3 (1)	55 (1)	292.892
9	20:1 (−1)	2 (0)	55 (1)	395.646
10	20:1 (−1)	1 (−1)	55 (1)	382.353
11	15:1 (0)	2 (0)	45 (0)	353.778
12	10:1 (1)	2 (0)	35 (−1)	358.661
13	15:1 (0)	2 (0)	45 (0)	359.775
14	15:1 (0)	1 (−1)	35 (−1)	277.137
15	15:1 (0)	2 (0)	45 (0)	338.412
16	15:1 (0)	3 (1)	35 (−1)	419.320
17	10:1 (1)	1 (−1)	45 (0)	328.890

The normal probability plot of the responses Y residuals is illustrated in Figure 8a. The residuals were distributed along an approximately straight line, which indicated that the error obeyed a normal distribution [71]. The correlation between the predicted and actual values (Figure 8b) clearly demonstrated agreement between the model's predicted values and the actual values of the experimental data. This indicated that there was a good fit between the actual values and the model predictions and showed that the preparation conditions for the medicated moxa sticks were appropriate. The order of influence of various factors on the Y responses (Table 6) was as follows: solid–liquid ratio (F = 35.95) > drying time (F = 16.39) > drying temperature (F = 2.59). The regression model was significant, with a p-value of < 0.05 [72]. The lack-of-fit term for the model had a p-value of 0.8989 (i.e., > 0.05), which indicated that the model was consistent with reality and suitable for analysis and prediction of the preparation process of medicated moxa sticks. The correlation coefficient was 0.9659, and the adjusted coefficient of determination was 0.9220. These values indicated that the model could account for 92.2% of the variation in the response value and demonstrated that the model closely approximated reality.

3.4 | RSM Variable Analysis

Figure 9 shows the interactions of the solid–liquid ratio and drying time on the Y values at three different drying temperature levels (−1, 0 and 1). When the drying temperature was at level−1, the effect of drying time on Y value was small regardless of the solid–liquid ratio (Figure 9a,a*). When the drying temperature was increased to level 0 and the solid–liquid ratio was moderate, the Y values increased with increases in the drying time. When the drying temperature at level 1, the Y values did not change with the drying time. This results suggest that drying times that are too short or too long affect the active ingredients as well as the tar concentration. An appropriate solid–liquid ratio and drying time are needed to increase in the concentrations of active ingredients and decrease the tar concentration.

Figure 10 shows the interaction of the solid–liquid ratio and drying temperature on the Y values at three drying time levels

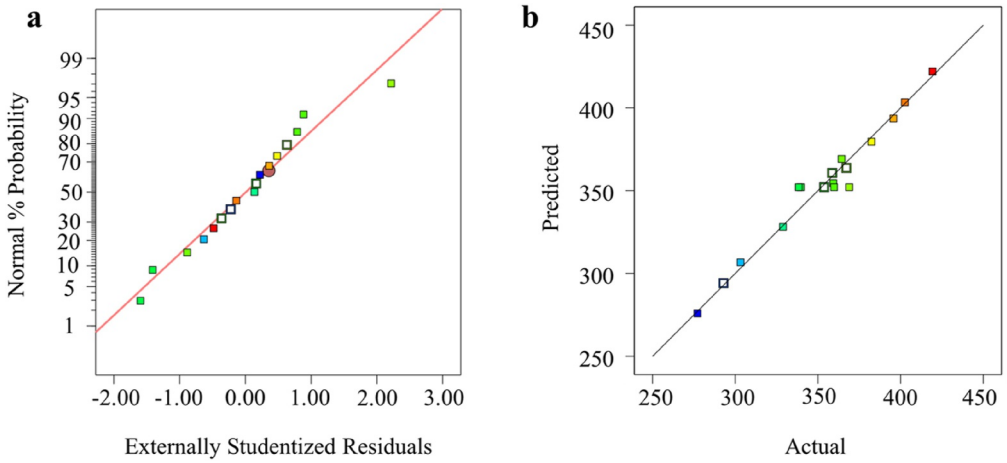

FIGURE 8 | Regression model of yield analysis: (a) normal plot of residuals and (b) comparison between the predicted and actual value.

TABLE 6 | Analysis of variance.

Source	Sum of squares	D_f	Mean square	*F*-value	*p*-value	Significant
Model	22,265.46	9	2473.94	22.02	0.0002	**
X_1	4037.70	1	4037.70	35.95	0.0005	**
X_2	1840.94	1	1840.94	16.39	0.0049	*
X_3	290.54	1	290.54	2.59	0.1518	
X_1 X_2	15.32	1	15.32	0.1363	0.7229	
X_1 X_3	1757.55	1	1757.55	15.65	0.0055	*
X_2 X_3	13,414.84	1	13,414.84	119.43	< 0.0001	**
X_1^2	655.35	1	655.35	5.83	0.0464	*
X_2^2	2.63	1	2.63	0.0234	0.8827	
X_3^2	295.71	1	295.71	2.63	0.1487	
Residual	786.28	7	112.33			
Lack of fit	97.51	3	32.50	0.1888	0.8989	
Pure error	688.77	4	172.19			
Correlation total	23,051.74	16				

Note: $R^2 = 0.9659$; $R_{adj}^2 = 0.9220$.
*$p < 0.05$.
**$p < 0.001$.

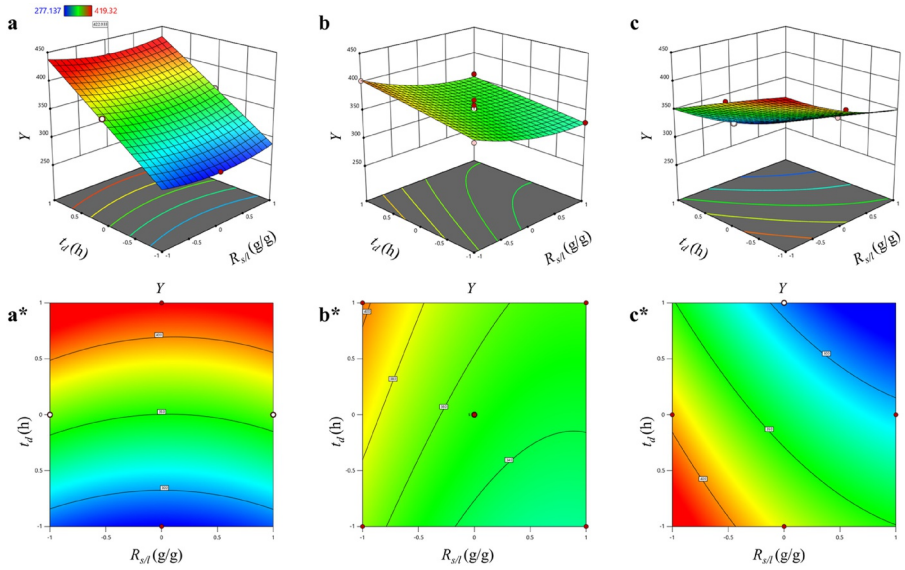

FIGURE 9 | (a), (b) and (c) Three-dimensional of effects of the interactions between X_1 and X_2 on Y at three X_3 levels (−1, 0 and 1). (a*), (b*) and (c*) Contours of the effects of the interactions between X_1 and X_2 on Y at the three levels of X_3 (−1, 0 and 1).

(−1, 0 and 1). When the drying time was at level−1, the Y values were greatly affected by the solid–liquid ratio. However, when the drying time was increased to level 0, the effects of the solid–liquid ratio and drying temperature on the Y values were only moderate. When the drying time was increased to level 1, the effects of the solid–liquid ratio and drying temperature on the Y values were minimal. The results showed that the best Y values were obtained with a moderate drying temperature.

Figure 11 shows the effects of the interactions of drying time and drying temperature on the Y values at three solid–liquid ratios (−1, 0 and 1). At level−1 and level 0, the Y values increased with the drying time and drying temperature. However, when the solid–liquid ratio was at level 1, the Y values were less affected by the drying temperature but increased as the drying time increased. These changes were attributed to the high drying temperature causing volatilisation of the active ingredients, which led to a decrease in the Y values.

3.5 | Verification the Optimum Conditions

The optimum conditions to prepare the medicated moxa sticks were a solid–liquid ratio of 15 g/g, a drying time of 3 h and a drying temperature of 35°C (Table 7). Under these conditions, the predicted Y value was 422.033. To verify the reliability of the

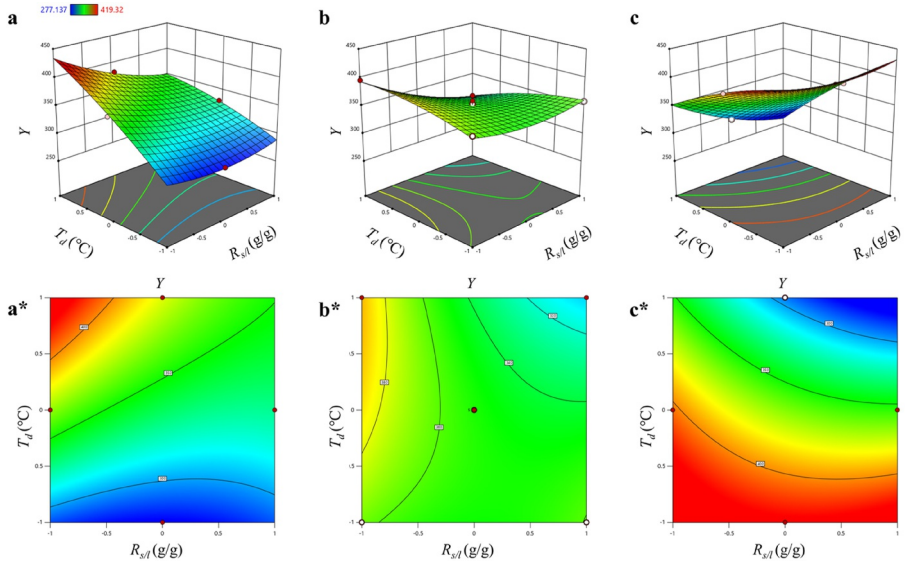

FIGURE 10 | (a), (b) and (c) Three-dimensional surfaces of the effects of the interaction between X_1 and X_3 on Y at three X_2 levels (−1, 0 and 1). (a*), (b*) and (c*) Contours of the effects of the interactions between X_1 and X_3 on Y at three levels of X_2 (−1, 0 and 1).

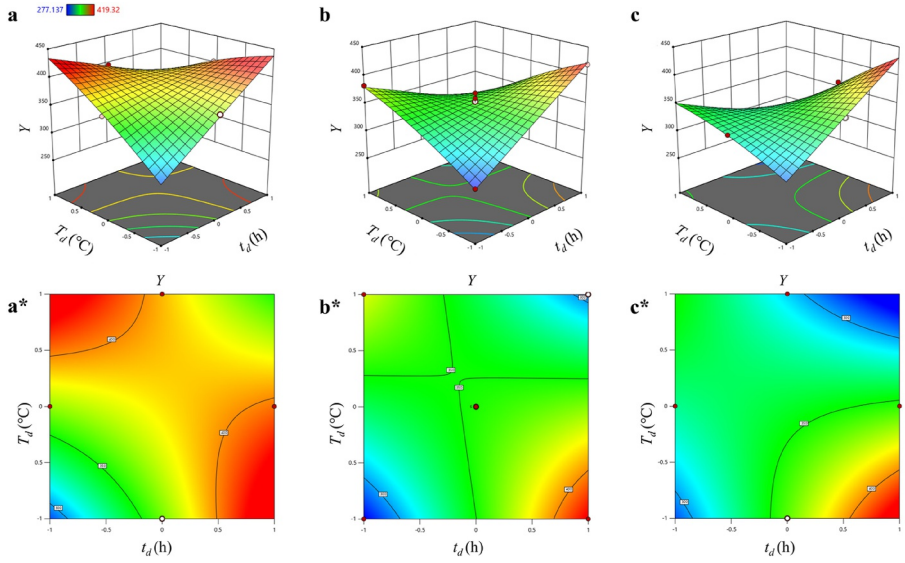

FIGURE 11 | (a), (b) and (c) Three-dimensional surfaces of the effects of the interaction between X_2 and X_3 on Y at three X_1 levels (−1, 0 and 1). (a*), (b*) and (c*) Contours of the effects of the interaction between X_2 and X_3 on Y at three levels of X_1 (−1, 0 and 1).

TABLE 7 | Optimum conditions and validation results.

			Y		
$R_{s/l}$ (g/g)	t_d (h)	T_d (°C)	Predicted	Experimental	Standard deviation
15	3	35	422.033	420.586	0.724

experimental results, the experiment was repeated under the same conditions and the measured value of Y was 420.586. The standard deviation between the predicted and experimental values was approximately 0.724, which indicated that the RSM model had good validity and reliability. Under these optimum conditions, the active ingredients content was 7.1%, which was made up of 0.3% terpineol, 0.4% borneol, 1.7% camphor, 0.1% ligustilide, 4.2% d-limonene and 0.4% cineole. The total content of active ingredients in the medicated moxibustion smoke was 34 times that in the pure moxibustion smoke. The tar concentration was 16.7 mg/g, which was lower than the Chinese national standard.

3.6 | Comparison of the Tar Concentration

The tar concentration produced by burning four types of moxa sticks were determined (Table 8). Among the moxa sticks tested,

the medicated moxa sticks prepared in this study had the lowest tar concentration. The use of Huangjiu during preparation of the medicated moxa sticks may have contributed to the low tar concentration. Huangjiu contains protease, which can effectively degrade the active ingredients in the moxa stick and reduce the amount of tar produced [65, 66]. In the Chinese national standard [73], the maximum allowable concentration of tar in moxa stick smoke is 45 mg/g. The tar concentration produced by burning the moxa sticks was lower than the standard for all four sticks tested; therefore, they all comply with the safety standard. However, the potential hazards of the tar should still be considered. Tar contains a variety of toxic polycyclic aromatic hydrocarbons [74], which pose a threat to human health. Therefore, because they have the lowest tar concentration, the medicated moxa sticks prepared in this study should be safer than the other moxa sticks tested.

3.7 | Transdermal Absorption Mechanism of Active Ingredients in Moxibustion Smoke

Figure 12a,b show the microscopic transdermal processes of the active ingredients in pure moxibustion smoke and medicated moxibustion smoke. Obvious molecular diffusion and adsorption behaviour can be observed in both systems during the dynamic process. In comparison, the medicated moxibustion smoke ingredients displays a higher degree of molecular aggregation at 1000 ps with a denser adsorption layer, whereas the molecular distribution of the pure moxibustion smoke is relatively loose. Moreover, the active ingredients in medicated moxibustion smoke exhibiting generally higher adsorption energy with the skin system compared to that of pure moxibustion smoke, indicating a stronger binding affinity between the active ingredients and the adsorption sites within the stratum corneum of the skin. These results demonstrate that the active ingredients from the medicated moxibustion smoke tend to form more stable interactions and show stronger adsorption behaviour with the skin interface. It further means that the medicinal components of the medicated moxibustion smoke are more likely to accumulate in the stratum corneum of the skin for transdermal diffusion. This provides direct molecular-level evidence for its better therapeutic effect in the future practical applications.

The density distribution curves in Figure 12c shows that the active ingredients of both moxibustion smoke formed a concentration peak around from 50 to 60 Å, with the peak of medicated moxibustion smoke ingredients being sharper and higher, indicating a more concentrated distribution of the active ingredients in this region. The mean square displacement curves

TABLE 8 | Tar concentrations in the moxa sticks.

Moxa stick	Tar concentration (mg/g)
Medicated moxa stick	16.7
Pure moxa stick	19.6
Anhui lvying (No. Z20184071)	24.1
Jiangsu Kangmei (No. Z32020252)	21.8
Chinese national standard (GB/T 40976-2021)	≤ 45.0

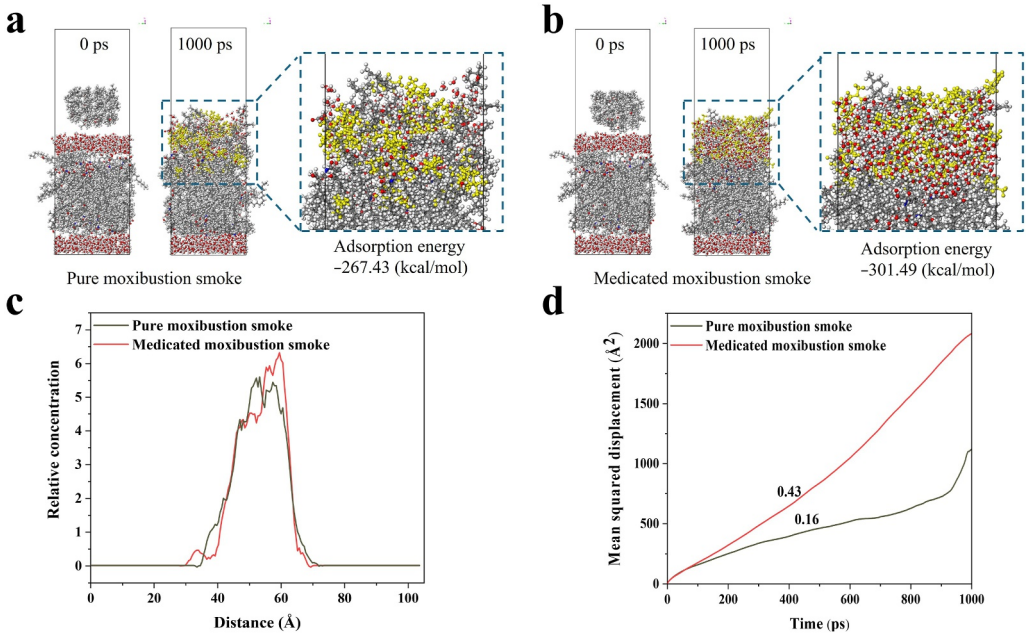

FIGURE 12 | Molecular dynamics simulation. Transdermal processes of the active ingredients in (a) pure moxibustion smoke and (b) medicated moxibustion smoke, (c) density distribution and (d) mean square displacement.

in Figure 12d shows that the diffusion coefficient of the active ingredients in medicated moxibustion smoke (0.43) was significantly higher than that in pure moxibustion smoke (0.16), indicating the stronger mobility within the diffusion system. Overall, the adsorption, concentration distribution and diffusion mobility of the active ingredients in medicated moxibustion smoke within the stratum corneum of the skin were enhanced, which might be help to improve the clinical efficacy.

3.8 | In Vitro Transdermal Experiments

The relationship between transdermal time and average fluorescence intensity of the active ingredients accumulated in the skin samples treated by moxibustion smoke was shown in Figure 13a. It can be seen that the average fluorescence intensity of the skin samples treated by both the pure and medicated moxibustion smoke increased as the transdermal time extended from 10 to 40 min, suggesting that the degree of transdermal penetration of active ingredients improved with longer application time. Moreover, the average fluorescence intensity of the skin treated by the medicated moxibustion smoke was consistently higher than that of the pure moxibustion smoke at each time point. It further confirms that the transdermal absorption efficiency of the active ingredients in the medicated moxibustion smoke is superior to that of the pure moxibustion smoke.

As shown in Figure 13b, the total contents of active ingredients in receiving solutions from pure moxibustion smoke and medicated moxibustion smoke were measured at 40 min, 2 h, 4 h, 6 h, 8 h and 12 h. In both groups, the content of active ingredients gradually increased over time, which indicated that the compounds accumulated after percutaneous permeation. Throughout the observation period, the content of active ingredients in the medicated moxibustion smoke receiving solution was much higher than that in the pure moxibustion smoke receiving solution. This showed that the components from medicated moxibustion smoke had superior transdermal permeation rates and total cumulative permeation amounts compared with those from pure moxa moxibustion smoke. The higher surface temperature of the skin induced by the medicated moxibustion smoke compared with that by the pure moxibustion smoke potentially accelerated the transdermal absorption rate of pharmacologically active components [75]. These results confirmed the medicated moxibustion smoke had enhanced transdermal delivery capacity compared with pure moxibustion smoke. The results also provide a reference for further evaluation of the ability of moxibustion smoke to promote transdermal absorption and enhance bioavailability of active components in practical applications.

3.9 | Experiments in Rats

Figure 14 shows the therapeutic effects of moxibustion with pure moxa sticks and medicated moxa sticks on toe swelling in a rat model of joint disease. It could be seen that the toe swelling of rats in all groups was significantly increased after modelling. Following moxibustion intervention, toe swelling of rats in both the pure and medicated moxa stick treatment groups was gradually reduced. On day 7, the toe swelling degree of rats in medicated moxa stick treatment group was significantly lower than that in the pure moxa stick treatment group and the model group. Morphological observations showed the obvious redness and swelling in the rat toes after modelling. The redness and swelling in the medicated moxa stick treatment group began to alleviate after one day moxibustion and the toe morphology almost returned to normal on day 7, whereas the improvement was much slower in the other two groups. These results indicated that moxibustion with medicated moxa sticks alleviated joint swelling more effectively than that of pure moxa sticks. The better therapeutic effect could be attributed to the enhanced anti-inflammatory and detumescent effects induced by the transdermal absorbed active ingredients in the medicated moxibustion smoke.

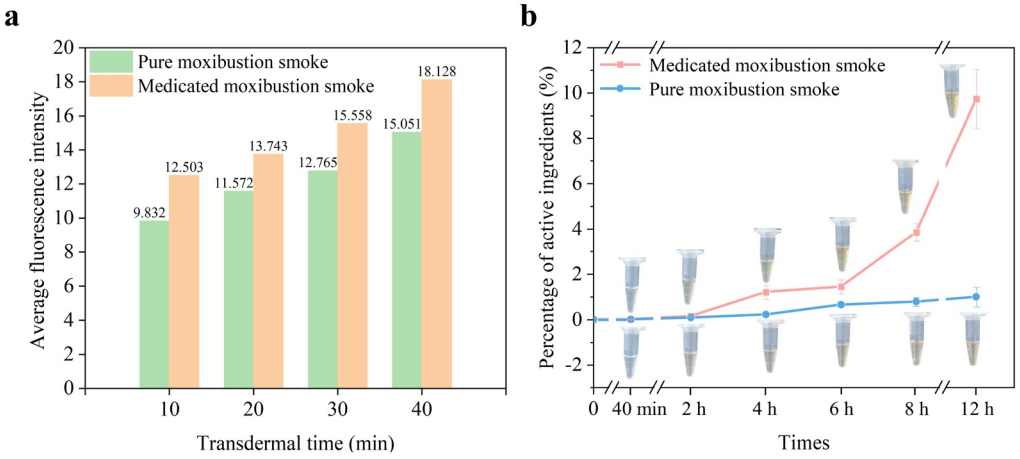

FIGURE 13 | Transdermal performance of active ingredients in pure and medicated moxibustion smoke. (a) Average fluorescence intensity of active ingredients accumulated in the skin samples treated by moxibustion smoke and (b) contents of active ingredients in receiving solutions obtained from moxibustion smoke.

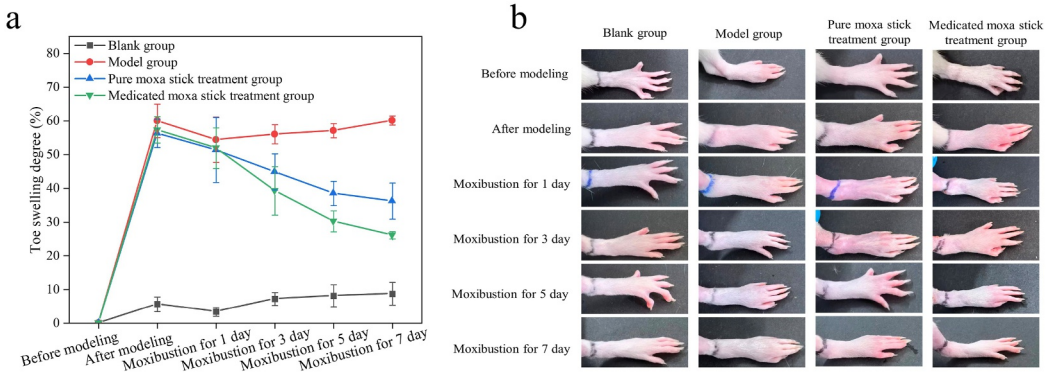

FIGURE 14 | Therapeutic effects of moxibustion with pure moxa sticks and medicated moxa sticks on toe swelling in a rat model of joint disease. (a) Changes in toe swelling degree and (b) photographs of toe morphology.

4 | Conclusions

In this study, the herbs in JBD was added to moxa wool to prepare medicated moxa sticks for joint disease. GC–MS was used to analyse the moxibustion smoke components. Network pharmacology and molecular docking were used to explore the pharmacological mechanisms for joint disease. A BBD was used to optimise the preparation process of the medicated moxa sticks. At the same time, molecular dynamics simulations were combined with animal experiments to verify its efficacy. The main conclusions were as follows.

1. Thirty-four more active ingredients were detected in smoke produced by medicated moxa sticks than that produced by pure moxa sticks. Network pharmacological predictions suggested that six active ingredients, terpineol, borneol, camphor, ligustilide, d-limonene, and cineole, were the most likely to modulate joint disease through the TNF signalling pathway. The results of molecular docking validation demonstrated that favourable binding interactions existed between these active ingredients and their target proteins. It demonstrated the potential of the medicated moxa sticks for multitargeted anti-inflammatory therapy for joint disease.
2. The total content of the six active ingredients in the medicated moxibustion smoke was 34 times to that in the pure moxa stick smoke. However, the tar concentration in medicated moxa sticks prepared under optimised conditions was 14.8% lower than that in pure moxa sticks and 30.7% lower than that in commercially available medicated moxa sticks. These indicate that the developed medicated moxa sticks are more environmentally friendly and effective for the treatment of joint disease than that of pure moxa sticks.
3. Molecular dynamics simulations and experiment in rats proved that the medicated moxa sticks outperformed pure moxa sticks in the cumulative of active ingredients in skin, transdermal penetration rate and detumescence efficacy, showing the good therapeutic effect of the develop medicated moxa sticks on joint diseases.

The developed medicated moxa sticks displayed good efficacy and environmental safety for the clinical treatment of joint disease. In future, a series of animal experiments will be used to fully assess the pharmacological effects and bioavailability of the active ingredients.

Acknowledgements

This work was funded by grants from the University-Enterprise Cooperative Project (Grant 2023HZ041), which was acknowledged gratefully. The authors thank the National Super-computing Center in Shenzhen for providing the computational resources.

Conflicts of Interest

The authors declare no conflicts of interest.

Data Availability Statement

The data that support the findings of this study are available from the corresponding author upon reasonable request.

References

1. J. M. Wen, Z. J. Zhuang, M. H. Zhao, et al., "Treatment of Poststroke Constipation With Moxibustion: A Case Report," *Medicine* 97, no. 24 (2018): e11134, https://doi.org/10.1097/MD.0000000000011134.

2. Y. F. Xie, L. Xiao, J. M. Zhang, et al., "Moxibustion and Fier Needle Acupuncture for Gouty Arthritis: A Systematic Review and Meta-Analysis," *Journal of Mechanics in Medicine and Biology* 24, no. 8 (2024): 2440055, https://doi.org/10.1142/S0219519424400554.

3. Y. M. Zhong, K. Luo, Y. D. Guo, X. H. Gao, and H. Y. Zhou, "Moxibustion Regulates the Expression of T Cells in Rheumatoid Arthritis Through Tim-3/Gal-9 Signaling Pathway," *Rejuvenation Research* 28, no. 1 (2025): 17–24, https://doi.org/10.1089/rej.2024.0052.

4. Y. Li, C. Sun, J. J. Kuang, et al., "An In Vitro and Numerical Study of Moxibustion Therapy on Biological Tissue," *IEEE Transactions on Biomedical Engineering* 65, no. 4 (2018): 779–788, https://doi.org/10.1109/TBME.2017.2719633.

5. F. Hao, Q. Wang, L. Liu, et al., "Effect of Moxibustion on Autophagy and the Inflammatory Response of Synovial Cells in Rheumatoid Arthritis Model Rats," *Journal of Traditional Chinese Medicine* 42, no. 1 (2022): 73–82, https://doi.org/10.19852/j.cnki.jtcm.20210324.002.

6. H. Kim, M. H. Kim, U. L. Choi, et al., "Molecular and Phenotypic Investigation on Antibacterial Activities of Limonene Isomers and Its Oxidation Derivative Against *Xanthomonas oryzae pv. Oryzae*," *Journal of Microbiology and Biotechnology* 34, no. 3 (2024): 562–569, https://doi.org/10.4014/jmb.2311.11016.

7. X. X. Wang, Y. Hou, L. Ding, et al., "Moxibustion for Anorexia in COVID-19," *Medicine* 101, no. 8 (2022): e28894, https://doi.org/10.1097/MD.0000000000028894.

8. X. Xu, M. M. Wang, Z. L. Sun, et al., "Discovery of Serum Proteomic Biomarkers for Prediction of Response to Moxibustion Treatment in Rats With Collagen-Induced Arthritis: An Exploratory Analysis," *Acupuncture in Medicine* 34, no. 3 (2016): 184–193, https://doi.org/10.1136/acupmed-2015-010909.

9. Y. Li, E. S. Hong, W. G. Ye, and J. Y. You, "Moxibustion as an Adjuvant Therapy for Cancer Pain: A Systematic Review and Meta-Analysis," *Journal of Pain Research* 16, no. 2 (2023): 515–525, https://doi.org/10.2147/JPR.S396696.

10. Y. G. Xia, R. Sun, Y. Y. Zhu, et al., "Moxibustion Treatment of COVID-19 and Rehabilitation Period of COVID-19: A Scoping Review," *Journal of Integrative and Complementary Medicine* 29, no. 10 (2023): 637–648, https://doi.org/10.1089/jicm.2022.0742.

11. Y. X. Peng, B. B. Lu, L. Li, et al., "External Treatment of Traditional Chinese Medicine for Myasthenia Gravis: A Protocol for Systematic Review and Meta-Analysis," *Medicine* 100, no. 15 (2021): e25475, https://doi.org/10.1097/MD.0000000000025475.

12. H. Butt, L. Nissim, L. Gao, C. Myant, G. de Boer, and R. Hewson, "Transient Mixed Lubrication Model of the Human Knee Implant," *Biosurface and Biotribology* 7, no. 4 (2021): 206–218, https://doi.org/10.1049/bsb2.12020.

13. A. C. T. Choh, A. Yew, S. J. Yeo, D. Y. R. Chong, and S. L. Chia, "Finite Element Analysis of Tibio-Femoral Contact Mechanics of a Customised Knee Spacer," *Biosurface and Biotribology* 8, no. 2 (2022): 121–128, https://doi.org/10.1049/bsb2.12035.

14. J. H. Chiu, "How Does Moxibustion Possibly Work?," *Evidence-Based Complementary and Alternative Medicine* 2013 (2013): 198584–198588, https://doi.org/10.1155/2013/198584.

15. X. R. Zhang, T. N. Li, Y. Y. Ren, et al., "The Important Role of Volatile Components From a Traditional Chinese Medicine Dayuan-Yin Against the COVID-19 Pandemic," *Frontiers in Pharmacology* 11, no. 9 (2020): 583651, https://doi.org/10.3389/fphar.2020.583651.

16. H. Shafaroodi, S. Roozbahani, and J. Asgarpanah, "The Essential Oil From Ferulago angulata (Schltdl.) Boiss. Fruits Exerting Potent Analgesic and Anti-Inflammatory Effects," *Journal of Physiology & Pharmacology* 72, no. 1 (2021): 81–87, https://doi.org/10.26402/jpp.2021.1.08.

17. M. Q. Shan, Y. L. Jiang, Y. Y. Fu, et al., "A Review of the Botany, Traditional Uses, Phytochemistry and Pharmacology of Nepeta tenuifolia Briq," *Phytochemistry Reviews* 20, no. 5 (2021): 991–1012, https://doi.org/10.1007/s11101-020-09729-x.

18. C. X. Ma, H. Fan, L. Dong, and Y. Zhou, "Treatment of Forty Cases of Knee Osteoarthritis of Cold-Dampness Arthralgia Type With Thunder Fire Moxibustion at Heat Sensitive Points," *Henan Traditional Chinese Medicine* 42, no. 12 (2022): 1913–1916, https://doi.org/10.16367/j.issn.1003-5028.2022.12.0403.

19. Y. H. Wang, Y. Zhou, Y. Z. Xie, et al., "The Effect of Ultrasound-Guided Acupotomy and Juanbi Decoction on Lumbar Disc Herniation: A Randomized Controlled Trial," *Medicine* 102, no. 1 (2023): e32622, https://doi.org/10.1097/MD.0000000000032622.

20. T. T. Wang, Q. Y. Jia, T. Chen, et al., "Alleviation of Synovial Inflammation of Juanbi-Tang on Collagen-Induced Arthritis and TNF-Tg Mice Model," *Frontiers in Pharmacology* 11, no. 2 (2020): 45, https://doi.org/10.3389/fphar.2020.00045.

21. Q. Wang, Y. R. Wang, Q. Y. Jia, et al., "The Efficacy of the Traditional Chinese Medicine Juanbi Pill Combined With Methotrexate in Active Rheumatoid Arthritis: Study Protocol for a Randomized Controlled Trial," *Trials* 19, no. 1 (2018): 188, https://doi.org/10.1186/s13063-018-2555-1.

22. H. L. Zhou, L. Y. Huang, K. J. Zhan, and X. D. Liu, "Wenhua Juanbi Recipe Attenuates Rheumatoid Arthritis via Inhibiting miRNA-146a-Mediated Autophagy," *BioMed Research International* 2022, no. 11 (2022): 1768052, https://doi.org/10.1155/2022/1768052.

23. W. P. Chan, S. A. M. B. Yusoff, A. Veksha, A. Giannis, T. Lim, and G. Lisak, "Analytical Assessment of Tar Generated During Gasification of Municipal Solid Waste: Distribution of GC-MS Detectable Tar Compounds, Undetectable Tar Residues and Inorganic Impurities," *Fuel* 268 (2020): 117348, https://doi.org/10.1016/j.fuel.2020.117348.

24. J. B. Li, C. Sun, A. J. Hou, et al., "Exploring Wine-Processing: A Distinctive Classic Technique in TCM," *RSC Advances* 15, no. 53 (2025): 45157–45176, https://doi.org/10.1039/d5ra05383h.

25. N. Yu, X. M. Zhu, S. S. Feng, et al., "A Breathable PTFE Membrane for Enhanced Moxibustion Process and Occupational Health Protection," *Journal of Membrane Science* 655, no. 8 (2022): 120579, https://doi.org/10.1016/j.memsci.2022.120579.

26. Y. F. Zhou, C. L. Wang, J. J. Kou, et al., "Chrysanthemi flos Extract Alleviated Acetaminophen-Induced Rat Liver Injury via Inhibiting Oxidative Stress and Apoptosis Based on Network Pharmacology Analysis," *Pharmaceutical Biology* 59, no. 1 (2021): 1378–1387, https://doi.org/10.1080/13880209.2021.1986077.

27. D. J. Wu, L. Hong, S. Y. Xu, et al., "Integrating Network Pharmacology and Experimental Validation via PPAR Signaling to Ameliorate Rheumatoid Arthritis: Insights From Corydalis Decumbentis Rhizoma (Xiatianwu)," *Fitoterapia* 183 (2025): 106541, https://doi.org/10.1016/j.fitote.2025.106541.

28. L. L. Pan, Z. Z. Li, Y. F. Wang, B. Y. Zhang, G. R. Liu, and J. H. Liu, "Network Pharmacology and Metabolomics Study on the Intervention of Traditional Chinese Medicine Huanglian Decoction in Rats With Type 2 Diabetes Mellitus," *Journal of Ethnopharmacology* 258 (2020): 112842, https://doi.org/10.1016/j.jep.2020.112842.

29. X. Q. Cao, S. Q. Zhang, M. J. Mao, Q. W. Zhang, and Y. Guo, "Exploring the Mechanism of Polygonum cuspidatum in the Treatment of Ischemic Stroke by Network Pharmacology Analysis and Experimental Validation," *Fitoterapia* 182 (2025): 106414, https://doi.org/10.1016/j.fitote.2025.106414.

30. X. Z. Wu, W. Li, Z. L. Luo, and Y. Z. Chen, "The Molecular Mechanism of Ligusticum wallichii for Improving Idiopathic Pulmonary Fibrosis: A Network Pharmacology and Molecular Docking Study," *Medicine* 101, no. 6 (2022): e28787, https://doi.org/10.1097/MD.0000000000028787.

31. Y. L. Li, S. J. Wang, Q. Wang, and M. Xing, "Enhancement of Fracture Properties of Polymer Composites Reinforced by Carbon Nanotubes : A Molecular Dynamics Study," *Carbon* 129 (2018): 504–509, https://doi.org/10.1016/j.carbon.2017.12.029.

32. B. Shao, L. X. Sun, N. Xu, H. W. Gu, H. Y. Ji, and L. H. Wu, "Development and Evaluation of Topical Delivery of Microemulsions Containing Adapalene (MEs-Ap) for Acne," *AAPS PharmSciTech* 22, no. 3 (2021): 125, https://doi.org/10.1208/s12249-021-01989-w.

33. M. C. Lu and J. W. Pang, "Effect of Moxibustion on TLR4/NF-κB Signaling Pathway in Synovial Tissues of Adjuvant Arthritis Rats," *Shanghai Journal of Acupuncture and Moxibustion* 40, no. 4 (2021): 491–497, https://doi.org/10.13460/j.issn.1005-0957.2021.03.0393.

34. F. Qi, Y. L. Li, K. Ai, X. Cai, X. Li, and L. Liu, "The Establishment and Evaluation of Adjuvant-Induced Arthritis in SD Rats," *Journal of Hunan University of Chinese Medicine* 36, no. 1 (2016): 23–26, https://doi.org/103969/j.issn.1674-070X.2016.01.005.

35. Z. M. Jiang, L. N. Zhao, L. B. Wu, M. J. Wang, L. Liu, and L. Hu, "Comparison of Suspended Moxibustion With Moxa Sticks of Different Diameters on the Expressions of TNF-α, IL-6 and IL-2 in Rheumatoid Arthritis Rats," *Shanghai Journal of Acupuncture and Moxibustion* 40, no. 7 (2021): 866–872, https://doi.org/10.13460/j.issn.1005-0957.2021.13.2002.

36. H. Huang, J. X. Zheng, N. J. Shen, et al., "Identification of Pathways and Genes Associated With Synovitis in Osteoarthritis Using Bioinformatics Analyses," *Scientific Reports* 8, no. 1 (2018): 10050, https://doi.org/10.1038/s41598-018-28280-6.

37. A. Wree, M. D. Mcgeough, M. E. Inzaugarat, et al., "NLRP3 Inflammasome Driven Liver Injury and Fibrosis: Roles of IL-17 and TNF in Mice," *Hepatology* 67, no. 2 (2018): 736–749, https://doi.org/10.1002/hep.29523.

38. S. R. Kim, S. Lee, S. H. Kim, et al., "SGLT2 Inhibition Modulates NLRP3 Inflammasome Activity via Ketones and Insulin in Diabetes With Cardiovascular Disease," *Nature Communications* 11, no. 1 (2020): 2127, https://doi.org/10.1038/s41467-020-15983-6.

39. R. Lu, X. J. Yu, S. Liang, et al., "Physalin a Inhibits MAPK and NF-κB Signal Transduction Through Integrin alphaVbeta3 and Exerts Chondroprotective Effect," *Frontiers in Pharmacology* 12 (2021): 761922, https://doi.org/10.3389/fphar.2021.761922.

40. Y. H. Lee and S. Bae, "Intercellular Adhesion Molecule-1 Polymorphisms, K469E and G261R and Susceptibility to Vasculitis and Rheumatoid Arthritis: A Meta-Analysis," *Cellular and Molecular Biology* 62, no. 12 (2016): 84–90, https://doi.org/10.14715/cmb/2016.62.12.15.

41. P. L. Chi, Y. C. Chuang, Y. W. Chen, C. C. Lin, L. D. Hsiao, and C. M. Yang, "The CO Donor CORM-2 Inhibits LPS-Induced Vascular Cell Adhesion Molecule-1 Expression and Leukocyte Adhesion in Human Rheumatoid Synovial Fibroblasts," *British Journal of Pharmacology* 171, no. 12 (2014): 2993–3009, https://doi.org/10.1111/bph.12680.

42. F. T. Korkmaz and D. E. Kerr, "Genome-Wide Methylation Analysis Reveals Differentially Methylated Loci That Are Associated With an Age-Dependent Increase in Bovine Fibroblast Response to LPS," *BMC Genomics* 18, no. 1 (2017): 405, https://doi.org/10.1186/s12864-017-3796-1.

43. H. H. Wu, Y. L. Li, N. J. Liu, Z. Yang, X. M. Tao, and Y. P. Du, "TCF7L2 Regulates Pancreatic Beta-Cell Function Through PI3K/AKT Signal Pathway," *Diabetology & Metabolic Syndrome* 11, no. 1 (2019): 1–9, https://doi.org/10.1186/s13098-019-0449-3.

44. Z. Y. Fan, Y. H. Liu, Z. L. Shi, et al., "MiR-155 Promotes Interleukin-1beta-Induced Chondrocyte Apoptosis and Catabolic Activity by Targeting PIK3R1-Mediated PI3K/Akt Pathway," *Journal of Cellular and Molecular Medicine* 24, no. 15 (2020): 8441–8451, https://doi.org/10.1111/jcmm.15388.

45. S. M. I. Mahboubi Rabbani and A. Zarghi, "Selective COX-2 Inhibitors as Anticancer Agents: A Patent Review (2014-2018)," *Expert Opinion on Therapeutic Patents* 29, no. 6 (2019): 407–427, https://doi.org/10.1080/13543776.2019.1623880.

46. X. Y. Zhao, T. J. Wang, B. Cai, et al., "MicroRNA-495 Enhances Chondrocyte Apoptosis, Senescence and Promotes the Progression of Osteoarthritis by Targeting AKT1," *American Journal of Translational Research* 11, no. 4 (2019): 2232–2244, https://pmc.ncbi.nlm.nih.gov/articles/PMC6511756/.

47. Q. F. Wei, F. Lv, H. J. Zhang, et al., "MicroRNA-101-3p Inhibits Fibroblast-Like Synoviocyte Proliferation and Inflammation in Rheumatoid Arthritis by Targeting PTGS2," *Bioscience Reports* 40, no. 1 (2020): 20191136, https://doi.org/10.1042/BSR20191136.

48. M. H. Weisman, P. Durez, D. Hallegua, et al., "Reduction of Inflammatory Biomarker Response by Abatacept in Treatment of Rheumatoid Arthritis," *Journal of Rheumatology* 33, no. 11 (2006): 2162–2166, https://www.jrheum.org/content/33/11/2162.

49. P. A. Klimiuk, S. Sierakowski, I. Domyslawska, and J. Chwiecko, "Effect of Etanercept on Serum Levels of Soluble Cell Adhesion Molecules (sICAM-1, sVCAM-1, and sE-selectin) and Vascular Endothelial Growth Factor in Patients With Rheumatoid Arthritis," *Scandinavian Journal of Rheumatology* 38, no. 6 (2009): 439–444, https://doi.org/10.3109/03009740903079321.

50. L. Y. Zhang, X. X. Liang, Z. R. Ou, et al., "Screening of Chemical Composition, Anti-Arthritis, Antitumor and Antioxidant Capacities of Essential Oils From Four Zingiberaceae Herbs," *Industrial Crops and Products* 149, no. 7 (2020): 112342, https://doi.org/10.1016/j.indcrop.2020.112342.

51. K. X. Zhang, W. J. Liu, F. K. Shen, et al., "Ligustilide Covalently Binds to Cys703 in the Pre-S1 Helix of TRPA1, Blocking the Opening of Channel and Relieving Pain in Rats With Acute Soft Tissue Injury," *Journal of Ethnopharmacology* 330, no. 10 (2024): 118217, https://doi.org/10.1016/j.jep.2024.118217.

52. L. F. Hong, X. Li, Y. M. Bao, et al., "Preparation, Preliminary Pharmacokinetic and Brain Targeting Study of Metformin Encapsulated W/O/W Composite Submicron Emulsions Promoted by Borneol," *European Journal of Pharmaceutical Sciences* 133 (2019): 160–166, https://doi.org/10.1016/j.ejps.2019.03.019.

53. R. Ma, D. N. Lu, J. Wang, Q. Xie, and J. L. Guo, "Comparison of Pharmacological Activity and Safety of Different Stereochemical Configurations of Borneol: L-Borneol, D-Borneol, and Synthetic Borneol," *Biomedicine & Pharmacotherapy* 164, no. 8 (2023): 114668, https://doi.org/10.1016/j.biopha.2023.114668.

54. F. Anyakudo, E. Adams, and A. Van Schepdael, "Simultaneous Analysis of Volatile and Semi-Volatile Components in a Topical Formulation by Gas Chromatography Using a Programmed Temperature Vaporization Inlet and Flame Ionization Detection," *Journal of Pharmaceutical and Biomedical Analysis* 171, no. 7 (2019): 65–72, https://doi.org/10.1016/j.jpba.2019.03.057.

55. K. Végh, E. Riethmüller, A. Tóth, et al., "Convergence Chromatographic Determination of Camphor in the Essential Oil of Tanacetum Parthenium L," *Biomedical Chromatography* 30, no. 12 (2016): 2031–2037, https://doi.org/10.1002/bmc.3781.

56. E. Dar, A. Mobashar, A. Shabbir, et al., "Therapeutic Potential of d-Limonene in Rheumatoid Arthritis: Modulation of Inflammatory, Anti-Inflammatory Cytokines, and Prostaglandin E2," *Archiv Der Pharmazie* 357, no. 12 (2024): e2400388, https://doi.org/10.1002/ardp.202400388.

57. K. Preljevic, I. Pasic, M. Vlaovic, et al., "Comparative Analysis of Chemical Profiles, Antioxidant, Antibacterial, and Anticancer Effects of Essential Oils of Two Thymus Species From Montenegro," *Fitoterapia* 174 (2024): 105871, https://doi.org/10.1016/j.fitote.2024.105871.

58. M. D. S. Costa, J. E. Rocha, F. F. Campina, et al., "Comparative Analysis of the Antibacterial and Drug-Modulatory Effect of d-Limonene Alone and Complexed With Beta-Cyclodextrin," *European Journal of Pharmaceutical Sciences* 128 (2019): 158–161, https://doi.org/10.1016/j.ejps.2018.11.036.

59. Y. M. Zhu, F. J. Zuo, H. Z. Ouyang, et al., "Determination of Eleven Components in Rat Plasma by UPLC-MS/MS and GC-MS for Pharmacokinetic Studies After Oral Administration of Citri Reticulatae Pericarpium Extract," *Journal of Pharmaceutical and Biomedical Analysis* 248, no. 9 (2024): 116315, https://doi.org/10.1016/j.jpba.2024.116315.

60. E. A. A. El-Ghffar, O. A. Eldahshan, A. Barakat, and T. Efferth, "The Prophylactic Effect of a Eugenia Aquea Extract Against Oxidative Stress and Inflammation Associated With the Development of Arthritis in an Adjuvant-Induced Arthritis Rat Model," *Food & Function* 9, no. 12 (2018): 6644–6652, https://doi.org/10.1039/c8fo01570h.

61. C. Y. Li, C. G. Zhao, Y. Ma, et al., "Optimization of Ultrasonic-Assisted Ultrafiltration Process for Removing Bacterial Endotoxin From Diammonium Glycyrrhizinate Using Response Surface Methodology," *Ultrasonics Sonochemistry* 68, no. 11 (2020): 105215, https://doi.org/10.1016/j.ultsonch.2020.105215.

62. W. Z. Yan, J. Wang, Y. M. Wang, Y. H. Zeng, C. F. Chi, and B. Wang, "Optimization of the Preparation Process and Ameliorative Efficacy in Osteoporotic Rats of Peptide-Calcium Chelates From Skipjack Tuna (Katsuwonus pelamis) Meat," *Foods* 13, no. 17 (2024): 2778, https://doi.org/10.3390/foods13172778.

63. X. D. Yu, Z. F. Luo, D. Q. Gan, and G. M. Li, "Upgrading of Lignite Using a Combined Novel Drying and the FGX Dry Separation Process," *International Journal of Coal Preparation and Utilization* 41, no. 5 (2021): 343–361, https://doi.org/10.1080/19392699.2018.1477766.

64. W. T. Zhang, W. Duan, G. L. Huang, and H. L. Huang, "Ultrasonic-Assisted Extraction, Analysis and Properties of Mung Bean Peel Polysaccharide," *Ultrasonics Sonochemistry* 98, no. 6 (2023): 106487, https://doi.org/10.1016/j.ultsonch.2023.106487.

65. C. Liu, Y. Degrandpre, A. Porter, et al., "The Use of a Novel Tobacco Treatment Process to Reduce Toxicant Yields in Cigarette Smoke," *Food and Chemical Toxicology* 49, no. 9 (2011): 1904–1917, https://doi.org/10.1016/j.fct.2011.02.015.

66. P. B. Yu, J. Du, C. L. Cao, et al., "Development of a Novel Multi-Strain Wheat Qu With High Enzyme Activities for Huangjiu Fermentation," *Journal of the Science of Food and Agriculture* 101, no. 11 (2021): 4808–4817, https://doi.org/10.1002/jsfa.11127.

67. J. Zhang, B. Wang, G. L. Zhu, et al., "Optimization of the Integrated Processing Technology of Primary Processing for Asparagi Radix by HPLC-CAD Combined With the Box-Behnken Design," *Pharmacognosy Magazine* 19, no. 4 (2023): 937–945, https://doi.org/10.1177/09731296231191375.

68. O. Rodriguez, V. Eim, C. Rossello, A. Femenia, J. A. Carcel, and S. Simal, "Application of Power Ultrasound on the Convective Drying of Fruits and Vegetables: Effects on Quality," *Journal of the Science of Food and Agriculture* 98, no. 5 (2018): 1660–1673, https://doi.org/10.1002/jsfa.8673.

69. X. X. Sun, Z. S. Tang, Z. X. Song, J. N. Duan, and C. L. Wang, "Effects of Different Drying Methods on the Contents of Active Ingredients of Saposhnikovia divaricata (Turcz.) Schischk and Optimization of the Drying Process by Response Surface Methodology," *Phytochemical Analysis* 35, no. 1 (2024): 17–27, https://doi.org/10.1002/pca.3269.

70. F. D. Sun, R. Tao, Q. Liu, H. Wang, and B. H. Kong, "Effects of Temperature and pH on the Structure of a Metalloprotease From Lactobacillus fermentum R6 Isolated From Harbin Dry Sausages and Molecular Docking Between Protease and Meat Protein," *Journal of the Science of Food and Agriculture* 101, no. 12 (2021): 5016–5027, https://doi.org/10.1002/jsfa.11146.

71. H. Majdi, J. A. Esfahani, and M. Mohebbi, "Optimization of Convective Drying by Response Surface Methodology," *Computers and Electronics in Agriculture* 156, no. 1 (2019): 574–584, https://doi.org/10.1016/j.compag.2018.12.021.

72. X. Liu, R. Wang, C. G. Wang, et al., "Graphene Oxide Assisted Solvent for Enhancing the Coupled Ultrasonic Extraction Process of Curcumin From Curcuma longa L," *Separation Science and Technology* 58, no. 10 (2023): 1761–1772, https://doi.org/10.1080/01496395.2023.2215401.

73. *Moxa Floss Used in Moxibustion. GB/T 40976-2021* (China Zhijian Publishing House, 2021).

74. Y. Sarikaya, N. D. Kahya, A. D. Pekdemir, and M. Onal, "Removing Tar and Nicotine From Mainstream Cigarette Smoke Using Sepiolite-Modified Filter Tips," *Clay Minerals* 55, no. 4 (2020): 375–382, https://doi.org/10.1180/clm.2021.7.

75. Z. Z. Weng, Q. Wei, C. Ye, et al., "Traditional Herb (Moxa) Modified Zinc Oxide Nanosheets for Quick, Efficient and High Tissue Penetration Therapy of Fungal Infection," *ACS Nano* 18, no. 6 (2024): 5180–5195, https://doi.org/10.1021/acsnano.3c13164.

Supporting Information

Additional supporting information can be found online in the Supporting Information section.

Supporting Information S1: bsb270018-sup-0001-suppl-data.docx.